Chapter 4: Spatiotemporal Self-Organization on a Ring with Asymmetrically Placed Reference Electrode

4.1 Introduction

Since the use of a Luggin-Haber capillary is a standard method in electrochemistry to minimize voltage drop through the electrolyte, an understanding of the impact of the placement of the reference electrode on the dynamics of the reaction studies (such as the stability of homogeneous states) is of particular importance. In electrochemical systems a close reference electrode proved to give rise to a rich abundance of patterns [34]. Most of the experiments, in which the impact of the position of the ring electrode on pattern formation was investigated, have been carried out with a symmetric setup; the reference electrode was placed on the axis of the ring electrode. In this geometry, the measured potential at the reference electrode in the electrolyte is influenced equally by every position on the ring electrode, it depends on the average double layer potential and the feedback is symmetric. However, if the system has an asymmetric geometry, in other words, the reference electrode is removed from the symmetrical axis of the ring electrode, positions at the working electrode that are closer to the reference electrode have a larger influence on the measured potential than those that are further away. The effect of the feedback in the symmetric condition is superimposed by an additional asymmetric effect.

In this work, we studied the effect of an asymmetrically placed RE in the bistable and oscillatory regime during the electrocatalytic oxidation of formic acid on a Pt ring electrode.

4.2 Experimental

The schematic diagram of the principal three-electrode arrangement is shown in Figure 4.1. A smooth polycrystalline Pt ring was used as working electrode (WE). A concentric platinized Pt wire ring used as the counter electrode (CE) was placed 80 mm above the working electrode. The tip of a Luggin-Haber capillary hosting a Hg/Hg_2SO_4, K_2SO_4 (sat'd) reference electrode (RE) was removed from the symmetrical axis. The RE was fixed near the position 6 and separated from the center of the ring electrode with a constant distance of 24 mm, r_{RE} = 1.2 (r_{RE} is the distance between the center of ring electrode and the RE position divided by the radius of ring electrode). The pulse electrode (PE) was a Pt wire sealed in a glass except for a 2 mm tip. It was positioned above the WE at a distance of about 1 mm.

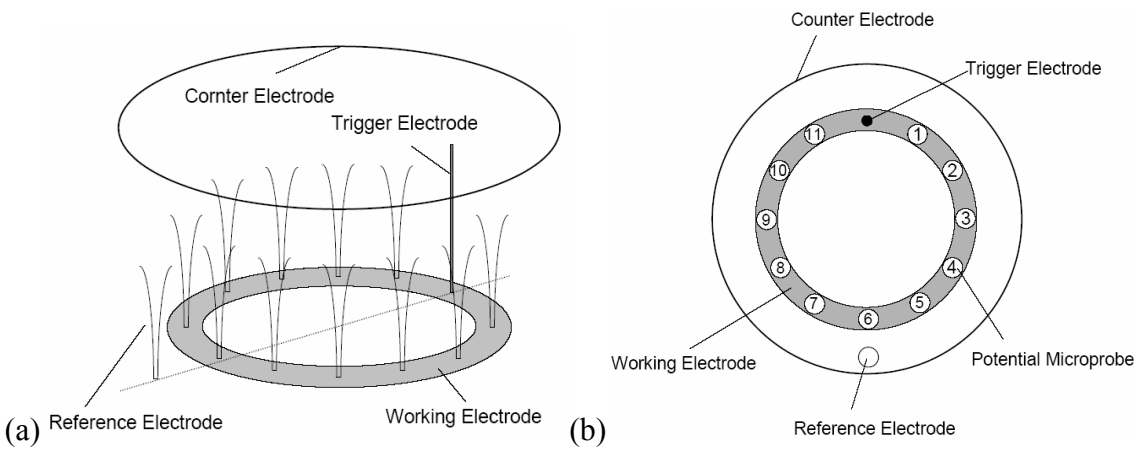

Figure 4.1. Schematic view of the electrode setup. (a) Reference electrode is placed outside the ring electrode. (b) Potential microprobes are separated by 30° angles and pulse electrode is placed at the position 12 of the ring electrode.

To detect the instantaneous local interfacial potentials on a Pt ring electrode, eleven microprobes were placed along the ring electrode close to the electrode surface (0.2 mm). Each microprobe capped with a Hg/Hg_2SO_4 electrode was filled with 0.5 M Na_2SO_4 solution (Merck, p.a.). All solutions were prepared with ultrapure water (Millipore Milli-Q water, 18 MΩ·cm) and were kept at room temperature. For investigation of the

electrocatalytic oxidation of formic acid, 0.1 M HCOONa (Merck, p.a.) in 0.033 M H_2SO_4 was used as the electrolyte. And we added 1×10^{-6} M bismuth ions (Bi^{3+}) into the main solution to reach oscillatory conditions. The electrolyte was extensively bubbled with N_2 before each experiment. A nitrogen atmosphere was maintained over the unstirred solutions during sweep experiments.

4.3 Experimental results

4.3.1 Perturbation in the bistable state

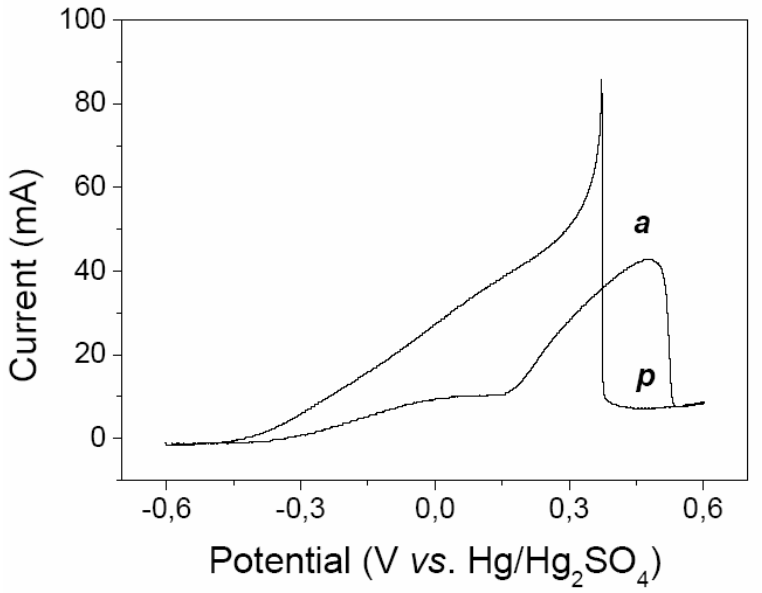

Figure 4.2 Cyclic voltammetry profile during the oxidation of formic acid on a Pt ring electrode with asymmetrically placed RE. 0.1M HCOONa / 0.033M H_2SO_4, R_{ext} = 5 Ω, scan rate 10 mV/s. ***a*** and ***p*** indicate the active and passive state.

Figure 4.2 displays the current-potential characteristic for the oxidation of formic acid during anodic and cathodic potential scans on a polycrystalline Pt ring electrode with a scan rate of 10 mV/s without bismuth ions. We added an external resistance (R_{ext} = 5 Ω), increasing the positive global coupling in order to suppress the occurrence of the stationary domains. On the anodic scan, the oxidation of formic acid increased gradually to high rate of direct oxidation of formic acid (active state). More anodically, oxygen-containing

species poisoned the surface and deactivated the ring electrode (PtOH) at +0. 530 V. On the cathodic scan, the electrode remained deactivated (passive state), and then a sharp and significant current peak appeared at +0.380 V. This was attributed to renewed oxidation of formic acid. Negative differential resistance and bistability were attributed to the formation of a deactive PtOH electrode [52]. However, a bistable regime was obtained between +0.380 V and +0.530 V, which was subjected to the comparative study of inhomogeneous surface potential on the ring electrode on two different states, *i.e.*, active (***a***) and passive state (***p***).

In electrodissolution systems front propagation phenomena can be traced back to the turn of the century [4], their first in-depth study in electroctalytic systems was recently undertaken by Flätgen *et al*. [13]; the authors investigated dynamical front patterns on a Ag ring electrode in the bistable region of the $S_2O_8^{2-}$ reduction system with the RE being placed far away from the WE. They observed locally triggered fronts which accelerated during the transition. Strasser *er al*. [18] described 'remote triggering' of travelling potential fronts; an additional passivation on one side of the already passive interface induced an almost immediate activation on the other. That is direct evidence of negative electrochemical coupling across the electrolyte.

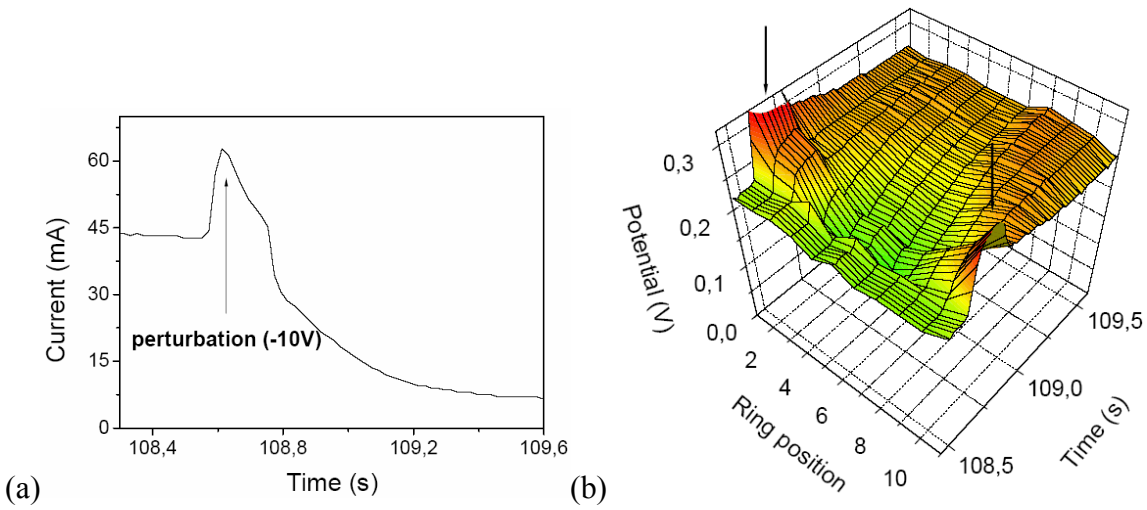

Figure 4.3. (a) Total current and (b) spatiotemporal distribution of interfacial potential during the negative potential perturbation. U = +0.494 V, R_{ext} = 5 Ω and U_{pulse} = -10 V (200 ms).

Passive/active transitions were performed with an asymmetrically placed RE in the bistable region using potential perturbations. In Figure 4.3, the total current and the pattern of interfacial potential along the electrode are shown as a function of time when a negative potential perturbation (-10 V, 200 ms) was applied to the active state of the bistable regime (+0.494 V) on the opposite position of the asymmetric RE. When the potential perturbation was applied, the current increased sharply and then decreased until the whole ring electrode had changed to the passive state (Figure 4.3(a)). And also, definitely, a passive front developed at the position where the perturbation was applied and spread along the ring electrode. So the state of ring electrode was changed to the passive state from the active state in Figure 4.3(b).

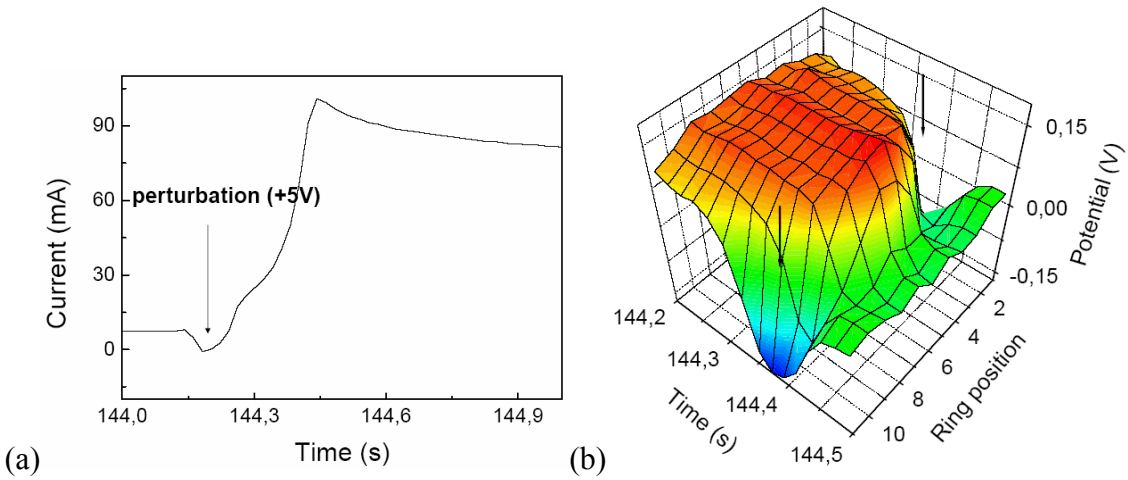

Figure 4.4. (a) Total current and (b) spatiotemporal distribution of local potential during the positive pulse potential was applied. U = +0.385 V, R_{ext} = 5 Ω and U_{pulse} = +5 V (200 ms).

When applying a positive potential perturbation (+5 V, 200 ms) on the opposite side of the asymmetric RE in the passive state of bistable regime (+0.385 V), the current increased sharply when the positive potential was applied because the surface of the ring electrode changed fast to the active state in Figure 4.4(a). The active front developed and travelled along the ring electrode till the surface of the ring electrode was changed to active state entirely in Figure 4.4(b). As earlier result [18], the application of a perturbation in the form of a positive potential caused the system to switch locally to the active state, and two activation fronts propagated along opposite directions of the ring.

4.3.2 Pattern formation in the oscillatory state

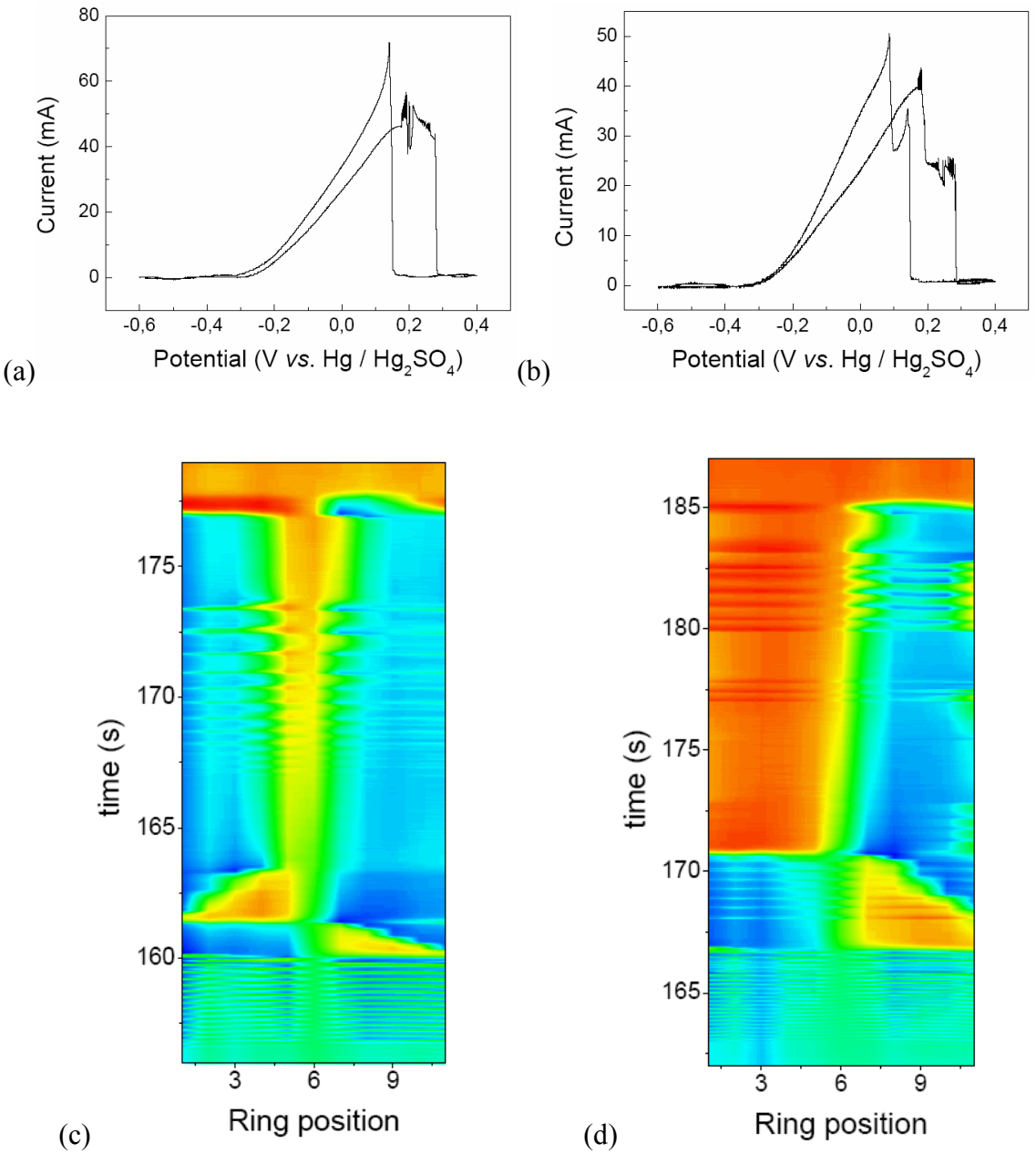

Figure 4.5. (a) and (c) cyclic voltammogram under same condition. (c) and (d) spatiotemporal pattern formations obtained during each voltammetric scan. Solution is 0.1 M HCOONa / 0.033 M H_2SO_4 /1×10^{-6} M bismuth ions, Scan rate is 5 mV/s, without external resistance.

Studies described in the following were carried out without external resistance. Figure 4.5 shows current oscillations and pattern formation of the interfacial potential during cyclic voltammetry with a scan rate of 5 mV/s. With the symmetric position of RE, oscillatory behavior was found to be reproducible for many successive scans. However, the asymmetric RE caused large irregular oscillations and a decrease in the stability and the reproducibility of the oscillatory states. During the current oscillations in Figure 4.5(a) and (b), various types of pattern formation of stationary domains (sD) and oscillations that consist of the active and passive state at the same time along the ring electrode could be obtained. In Figure 4.5(c), at the beginning of current oscillations, the distribution of the interfacial potential shows anti-phase oscillation patterns because of negative coupling (detailed descriptions will be shown). As the potential became higher, the large irregular oscillations were observed, and then the current oscillations disappeared for short terms at about 165 s. In these terms, stationary domains that had a strongly passive center on the position 6 and a strongly active state opposite the RE formed. These stationary domains were obtained very easily and are attributed to the strong effect asymmetric RE. Stationary domains were obtained at other positions during the cyclic voltammetry under the same conditions at 173 s in Figure 4.5(d); the passive state is the position 1-5, the active one is the position 7-11 of ring electrode.

Negative coupling can cause many complex spatiotemporal oscillation patterns that lead to change the system symmetrically and/or asymmetrically from the active to the passive state and back again [34]. In Figure 4.6, anti-phase and travelling pulses of interfacial potential are shown. During the cyclic voltammetry (scan rate 5 mV/s) period-2 current oscillations were observed in Figure 4.6(a), and spatiotemporal pattern formation was anti-phase wave (standing wave) in Figure 4.6(b). While one half of ring electrode exhibited strong activity, the other half of displayed a passive state due to the negative coupling. The position 6 near the RE was almost constant and appears as a kind of spatial node in the overall patterns. With a symmetric RE, first anti-phase oscillations were obtained, turning into travelling waves at higher potential although the latter should according to theory already coexist [21]. In contrast, in the present study no travelling pulses were observed during cyclic voltammetry, since anti-phase oscillations turned to complex large oscillations at higher potential. However, pulses could still be obtained by stopping the scan at not too high potential during anti-phase oscillations, which changed

into travelling waves over time. Current oscillations and its travelling pulse wave at low constant potential (+0.21 V) are shown in Figure 4.6(c) and (d). During the travelling pulse, the position 6 had high interfacial potential due to the effect of the RE ($u = E_0 + IR$).

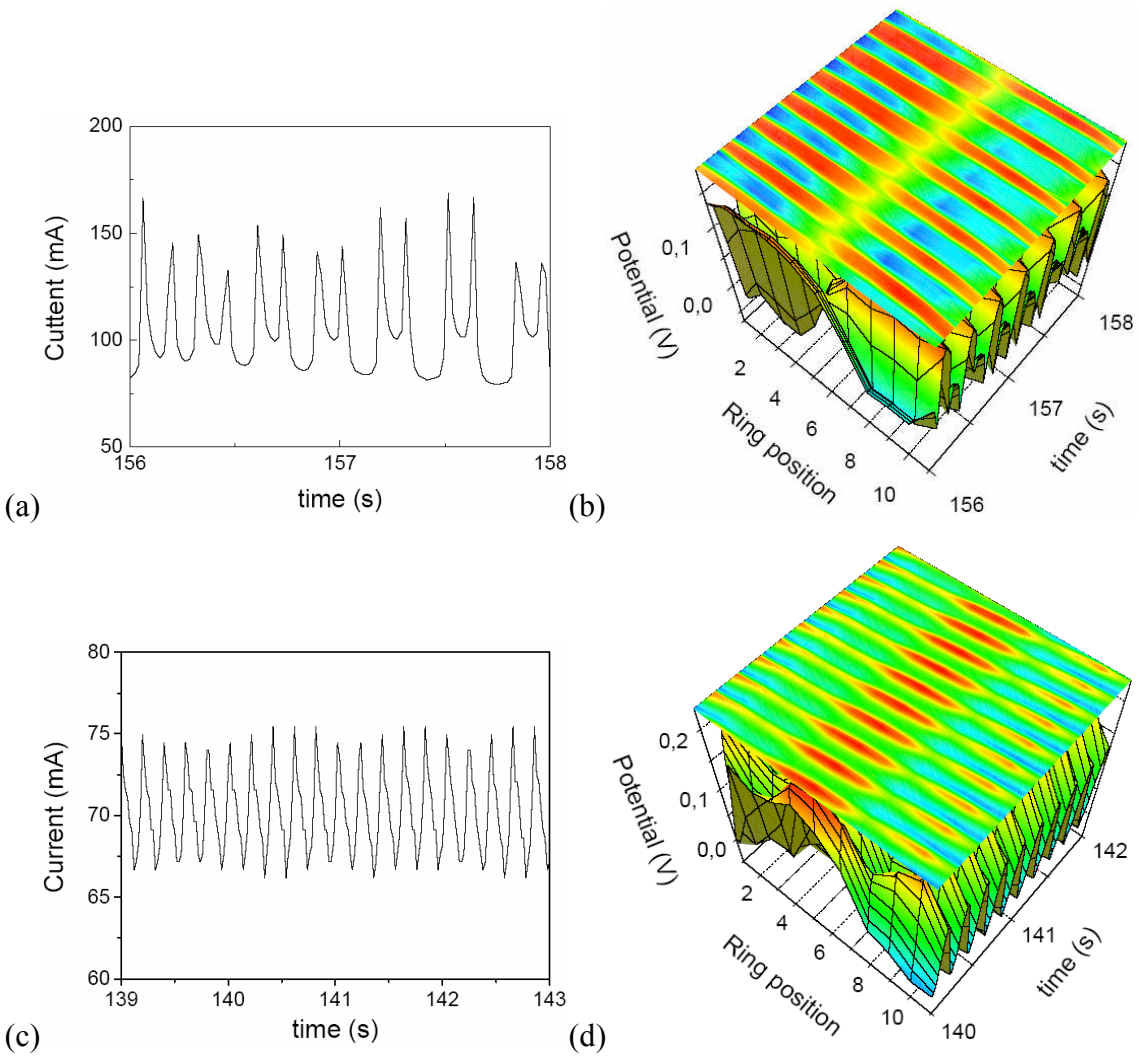

Figure 4.6. Spatiotemporal pattern formation during oscillations without external resistance; (a) current oscillations and (b) anti-phase pattern formation (during cyclic voltammetory at +0.186 V, scan rate: 5 mV/s), and (c) current oscillations and (d) travelling pulse pattern (at constant potential +0.21 V).

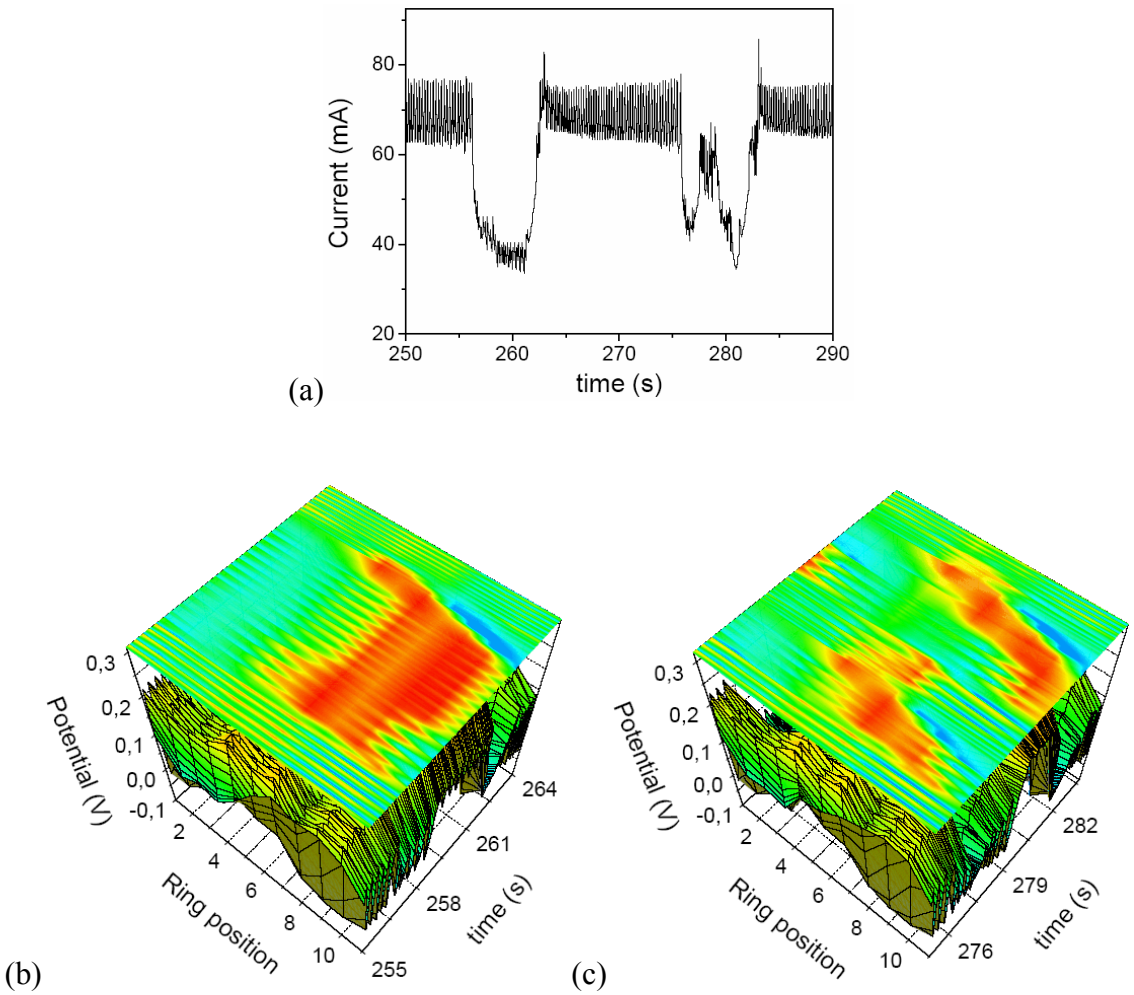

Figure 4.7. (a) Current oscillations at constant potential (+0.243 V), without external resistance, and various spatiotemporal patterns of asymmetric oscillation (b) and (c).

Moreover, various spatiotemporal patterns with a different passive center were observed, as shown in Figure 4.7. When a constant potential (+0.243 V) was applied, the current oscillations strongly decreased to low values in Figure 4.7(a). This was similar to the large irregular oscillations during cyclic voltammetry. When the current oscillations changed their form, the patterns changed also to standing wave that had strong passive state around the position 9 of the WE from the pulse waves in Figure 4.7(b), and also moving the strong passive state from the position 11 to 6 of the WE in Figure 4.7(c).

4.4 Discussion

When the RE is removed from the symmetrical axis and put near a position of the WE, the distribution of the double layer potential near the RE determines the measured potential Φ_{RE}. Then, Φ_{RE} will be given by $\Phi_{RE} \approx \Phi_0$ (Eq. (1.1) in chapter 1). Due to the potentiostatic condition, the space independent metal potential Φ_m depends on the RE potential, and also position at the WE that are close to the RE has a larger influence in Φ_{RE} than those that are farther away. So the asymmetric position of the RE creates an asymmetric feedback. Naturally, this should not matter in case of a spatially uniform distribution, but generally a close RE will lead to an inhomogeneous stationary domain or a spatial instability. Mathematically, this asymmetric feedback is described by a generalized equation [34].

$$\begin{aligned} C\frac{\partial u(x,t)}{\partial t} &= -i_r(u(x,t)) + \kappa h(x)(\Phi_m(t) - u(x,t)) \\ &\quad + \kappa\int_0^1 H_0(|x-x'|)(u(x',t)-u(x,t))\,dx' \\ &= -i_r(u(x,t)) + \frac{E_{eff}(t) - u(x,t)}{\rho_{tot}} \\ &\quad + \kappa\int_0^1 H_B(|x-x'|)(u(x',t)-u(x,t))\,dx' \end{aligned} \tag{4.1}$$

$$E_{eff} \approx E_0 - \int_0^1 \delta G_{RE}(x')\,u(x',t)\,dx' \tag{4.2}$$

$$\delta G_{RE}(x') \approx G_{RE}(r,\beta,x') - \langle G_{RE}(x')\rangle \tag{4.3}$$

E_{eff} is effective potential to include the asymmetric effect and δG_{RE} is the asymmetric part of Green's function. The squared brackets indicate the spatial average. $\delta G_{RE}(x')$ with $[\delta G_{RE}(x')] = 0$ has a maximum at the point of the electrode which is very close to the RE, and vanishes in the case of a symmetric position of the RE. The asymmetric part of the Green's function is shown for the asymmetric position of the RE at different radial distance r_{RE} (the

distance between the center of ring electrode and the RE position divided by the radius of ring electrode) in Figure 4.8.

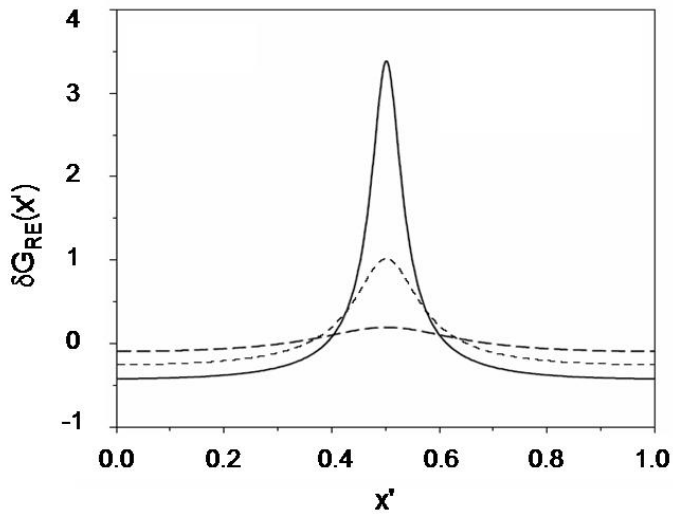

Figure 4.8. Asymmetric part of Green's function δG_{RE} (x') for the asymmetric RE at different radial distance r_{RE} (solid line: r_{RE} = 1.2, dot line: r_{RE} = 1.5, and dash line: r_{RE} = 2.5).

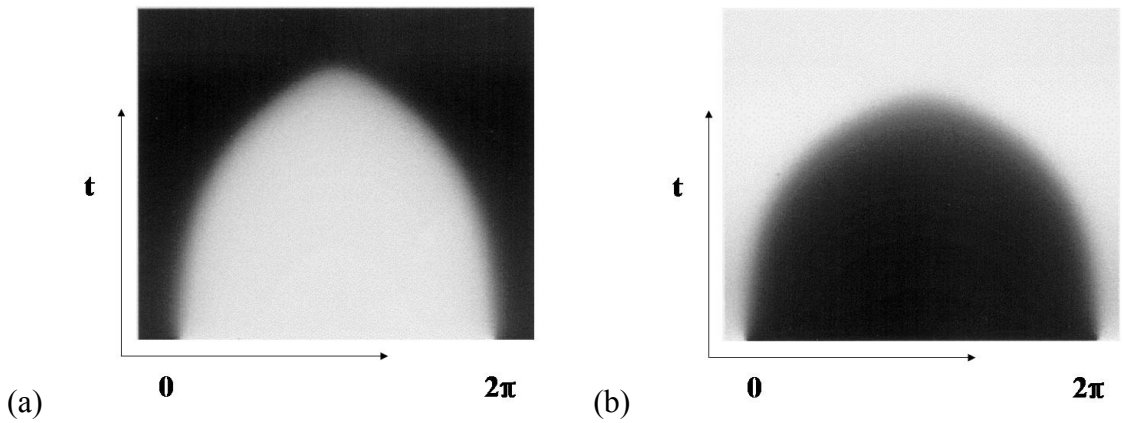

(a) (b)

Figure 4.9. Theoretical simulations of spatiotemporal dynamics. (a) passivation front induced by a passive perturbation at the opposite position of reference electrode (b) activation front triggered by active perturbation at the same place (white: active state, black: passive state). The perturbation was applied at position 0 = 2π [34].

Figure 4.9 shows that the theoretical simulation of spatiotemporal dynamics affected by asymmetric feedback. If the outer potential is fixed near the equistability, only front transitions leading to the more stable homogeneous phase should be expected. But if the electrode is in the active state and is given a passive perturbation at the opposite side of the RE, the double layer potential near the RE is low, then the measured potential Φ_{RE} which is determined by the active area near the RE will be high, so E_{eff}, respectively, Φ_m will be above the value of phase equistability. Consequently, two passive fronts develop and travel along the ring in Figure 4.9(a), in agreement with the experiment in Figure 4.3(b). But if the electrode is prepared in the passive state at the same parameters and an active perturbation is applied on the opposite side of the RE, the double layer potential on the position of the RE is high and the measured potential Φ_{RE} will be low, so that the effective potential E_{eff}, respectively, Φ_m will also be low and therefore below the value of phase equistability, thus enabling two activation fronts to develop in Figure 4.9(b), as in Figure 4.4(b). Therefore, it is no longer possible to distinguish between a metastable and a more stable phase, since sufficient fluctuations or perturbations on the opposite side of the ring will induce activation or passivation fronts. Stated differently, the asymmetric feedback leads to a quasi double-metastable behavior around the equistability line, even though it is a strictly one-component bistable system [35].

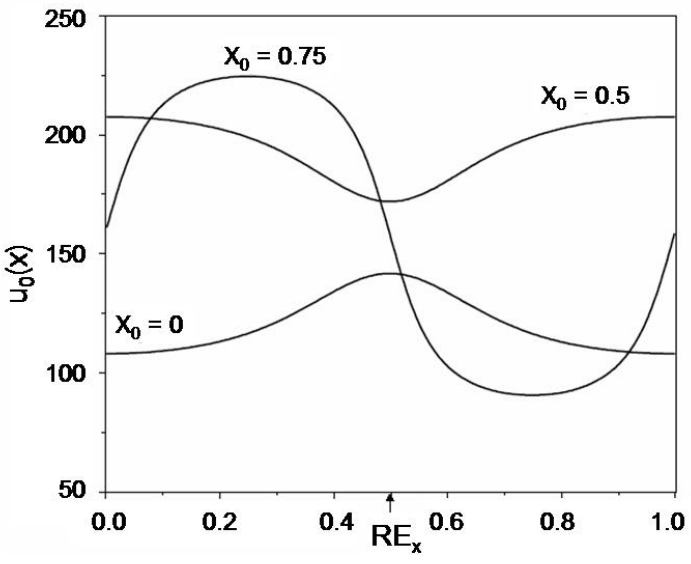

Figure 4.10. Theoretical simulation of three stationary domains with different location of potential minima x_0 (x_0 = 0, 0.5, and 0.75) [34].

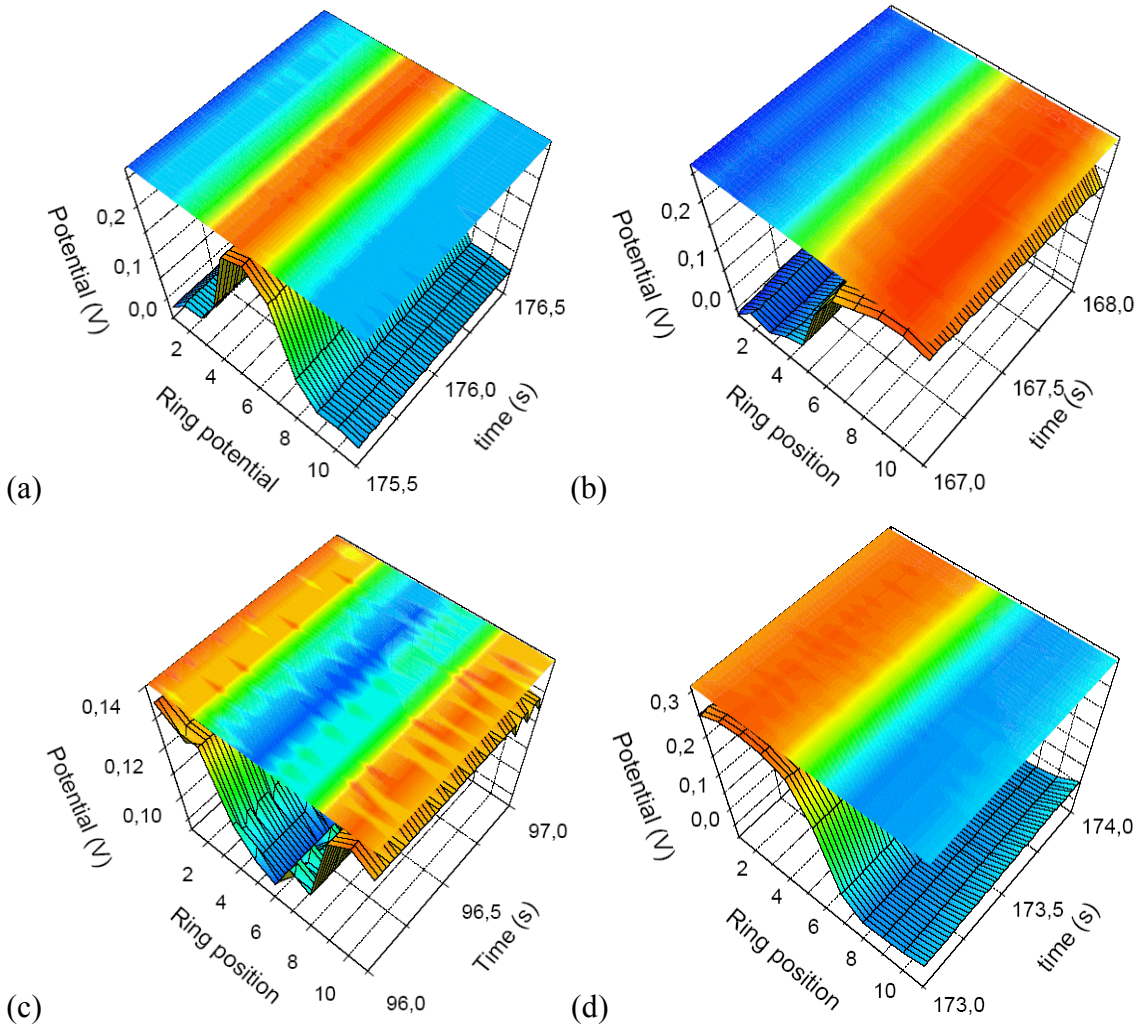

Figure 4.11. Several types of stationary domains (sD) with different location of potential minima x_0 during cyclic voltammetry without external resistance. (a) x_0 = 0, (b) x_0 = 0.25, (c) x_0 = 0.5 and (d) x_0 = 0.75.

One of the major effects of the asymmetric RE is the breaking of the translational invariance of the stationary domains (sD). Consider a stationary domain with the passive center located near the RE. Then, the measured potential will be small, therefore, the metal potential $\Phi_m = E_0 + \Phi_{RE}$ will be also small. Thus, the stationary domain consists of only a small passive part. If the stationary domain has its passive area on the opposite side of RE, the double layer potential on the position of the RE is low, Φ_{RE} and therefore Φ_m, will be high and the stationary domain will be mainly in the passive state with a small portion near the RE in a lower surface potential. As there are infinitely many solutions besides these two

depicted and as all of them are stable, consequently there are infinitely many different stationary values of the average double layer potential and of the total current, so that the experimentally measured current depends on the location of the nucleation, respectively, the position of the stationary domain and the experiment may therefore be regarded as irreproducible. Theoretical calculation of three stationary domains with a different passive center is shown in Figure 4.10, which is similar to the experiments in Figure 4.11. These are snapshots of quiescent phase during very complex dynamics, not directly comparable to the theoretical results on an idealized, noise-free bistable system.

Nevertheless the complex dynamics with sometimes prolonged quiescent phases persisted to potential values in cyclic voltammetry where the local dynamics should not be oscillatory any more (see Figure 4.5(b)). Therefore the poor reproducibility of the complex patterns may indeed be introductive of the coexistence of a large number of attractors with different relative stability and different domains of attraction, the transition between which can be triggered by fluctuations.